PET Quantification of Specific Binding of Carbon-11-Nicotine in Human Brain

Raymond F. Muzic, Jr., Marc S. Berridge, Robert P. Friedland, Ning Zhu and A. Dennis Nelson
Departments of Radiology, Biomedical Engineering, Chemistry and Neurology, Case Western Reserve University, Cleveland, Ohio

Previous work on the PET measured uptake of (S)-[^{11}C]nicotine presents conflicting findings as to whether it reflects specific binding. **Methods:** We studied the uptake of (R)-[^{11}C]nicotine and (S)-[^{11}C]nicotine in normal volunteers at baseline conditions and after a challenge with unlabeled (S)-nicotine to decrease the concentration of free binding sites or with CO_2 to increase perfusion. We analyzed the data using two- and three-compartment models. **Results:** We found tissue pharmacokinetics of (R)- and (S)-[^{11}C]nicotine are adequately described by the two-compartment model. (S)-nicotine challenge induced small but statistically significant reductions in distribution volume (DV) of both (R)- and (S)-[^{11}C]nicotine. The changes in DV could not be attributed to perfusion changes because DV was not affected by CO_2 challenge. Although the reduction in DV indicates sensitivity of [^{11}C]nicotine to status of nicotinic binding sites, the small magnitude of the reduction suggests that most nicotine uptake is nonspecific. **Conclusion:** Although differences in DV attributable to specific binding were detected, (R)- and (S)-[^{11}C]nicotine are relatively poor tracers for studying nicotinic binding sites using PET.

Key Words: PET; nicotine; nicotinic binding sites; specific binding
J Nucl Med 1998; 39:2048–2054

There is significant interest in the uptake and biodistribution of nicotine in the brain, because nicotine is a commonly used drug and because changes in nicotinic binding sites occur in Alzheimer's and Parkinson's diseases (*1*). Whereas an increase in the concentration of (S)-nicotine binding sites has been correlated with tobacco smoking in postmortem human brain tissue (*2*), a reduction in the number of these binding sites has been reported in in vitro studies of Alzheimer's and Parkinson's diseased brains (*3–7*). The relationship between cigarette smoking and these diseases is of special interest because it has been suggested that nicotine may have a protective effect against the development of Alzheimer's and Parkinson's diseases in humans (*8*).

These findings provide motivation to establish in vivo methods for studying and quantifying nicotine uptake and nicotinic binding sites in the brains of patients and human subjects. Långström et al. (*9*) and Halldin et al. (*10*) have labeled nicotine with ^{11}C, a positron-emitting isotope, and Nordberg et al. (*11–13*), Nybäck et al. (*14,15*) and Halldin et al. (*10*) have imaged its biodistribution in the human brain using PET. There is some question, however, as to whether the PET data were reflective of specific binding of nicotine. Nordberg et al. (*16*) analyzed their (S)-[^{11}C]nicotine data using a two-compartment kinetic model. They estimated values of the model parameters K_1 and k_2 and a composite parameter k_2^*, which is defined as k_2 normalized by the K_1 rate constant for [^{11}C]butanol. They found that k_2^* was negatively correlated with Mini-Mental State Examination score and that k_2^* was higher in temporal cortex, frontal cortex and hippocampus of Alzheimer's patients compared to controls. These results were interpreted as evidence of specific binding of (S)-[^{11}C]nicotine and not of changes in perfusion, since normalization by the K_1 rate constant is equivalent to normalization by cerebral blood flow because the single-pass extraction of butanol is high (*17,18*). However, this evidence was indirect because it was not demonstrated that k_2^* necessarily reflects (S)-[^{11}C]nicotine binding capacity. Two considerations in particular lead us to question this interpretation of the data. First, to minimize the effects of radioactive metabolites in the blood that were not measured, they made the PET experiments short, 4–5 min. This could render the data rather insensitive to specific binding. Second, Nybäck et al. (*15*) reported that the brain uptake of [^{11}C]nicotine is mainly related to perfusion and extraction across the blood–brain barrier and not to specific binding, because uptake of (S)-[^{11}C]nicotine was unaffected by 1 mg unlabeled nicotine administered concomitantly with or 7 min after (S)-[^{11}C]nicotine. Thus, it remains an unanswered question as to whether the PET-measured uptake of (S)-[^{11}C]nicotine represents specific binding. Because the (R) enantiomer of [^{11}C]nicotine has also been used in PET (*10–15*), the same question occurs regarding its biodistribution. Accordingly, the purpose of this study was to determine if there is any PET-observable specific uptake of (R)- or (S)-[^{11}C]nicotine and to devise a quantitative index of specific uptake that is independent of perfusion.

MATERIALS AND METHODS

General

[^{15}O]Butanol and (S)- or (R)-[^{11}C]nicotine uptake were imaged using an ECAT EXACT scanner (CTI, Knoxville, TN) (*19*) in normal volunteers. Catheters were placed in the radial artery and a contralateral arm vein for blood sampling and tracer injection, respectively. Written informed consent was obtained from volunteers who were paid to participate in the study that was approved by the Institutional Review Board, the Radiation Safety Committee, and the Radioactive Drug Research Committee of University Hospitals of Cleveland.

In five subjects, data were collected at baseline and beginning approximately 5 min after (S)-nicotine challenge. (S)-nicotine challenge consisted of intravenous administration of up to 2 mg unlabeled (S)-nicotine dissolved in saline solution and infused slowly until all the (S)-nicotine had been delivered or until the subject felt a moderate level of nausea. In two of these five subjects, [^{11}C]nicotine scans were collected using (R)-[^{11}C]nicotine and in three subjects the [^{11}C]nicotine scans were collected using (S)-[^{11}C]nicotine. As a control for perfusion effects, [^{15}O]butanol and (S)-[^{11}C]nicotine data were collected in three subjects at baseline and during CO_2 challenge. For this challenge, which was selected to increase cerebral perfusion (*18*), the subjects breathed 6% CO_2 beginning 4 min before each tracer injection and continuing to the end of the [^{15}O]butanol data acquisition or until 15 min into the [^{11}C]nicotine data acquisition. Volunteers were allowed to

Received Dec. 1, 1997; revision accepted Mar. 24, 1998.
For correspondence or reprints contact: Raymond F. Muzic, Jr., PhD, Division of Nuclear Medicine, University Hospitals of Cleveland, Cleveland, OH 44106.

TABLE 1
Abbreviations for Region of Interest Names

Name	Abbreviation
Caudate	caud
Cerebellar cortex	cbellar ctx
Inferior medial temporal cortex	inf med temp ctx
Inferior temporal cortex	inf temp ctx
Lateral frontal cortex	lat fr ctx
Lentiform nucleus	lent n
Lateral occipital cortex	lat occ ctx
Superior frontal cortex	sup fr ctx
Superior parietal cortex	sup par ctx
Medial frontal cortex	med fr ctx
Medial superior frontal cortex	med sup fr ctx
Medial occipital cortex	med occ ctx
Corona radiata (white matter)	cr wmat
Pons	pons
Thalamus	thal

rest and breathe room air for 10 min between the two scans. In all cases, time delay between baseline and challenge studies was sufficient so that the amount of (S)- or (R)-[^{11}C]nicotine remaining from the baseline scan was negligible during the challenge scans.

Data Collection

[^{15}O]Butanol. After bolus injection of 2.2 GBq (60 mCi) [^{15}O]butanol (*18*), PET data were collected into 18 × 5 sec frames for a total of 90 sec. Simultaneously, arterial blood radioactivity concentration was measured using a continuous-flow blood monitor (*20*).

[^{11}C]Nicotine. (R)- and (S)-nicotine were prepared according to Halldin et al. (*10*). An intravenous bolus of approximately 550 MBq (15 mCi) no-carrier-added [specific activity >12 GBq/μmol (320 mCi/μmol)] (S)- or (R)-[^{11}C]nicotine was administered approximately 15 min after [^{15}O]butanol administration to permit sufficient decay of the [^{15}O]butanol. PET data were collected into 12 × 10 sec, 9 × 20 sec, 5 × 60 sec and 4 × 300 sec frames for a total of 30 min. For the first 1.5 min, arterial blood radioactivity concentration was measured using a continuous-flow blood monitor (*20*). For the remaining duration, aliquots of arterial blood were withdrawn manually by a syringe at approximately 1.7, 3, 5, 7, 10, 15, 20 and 30 min postinjection. These samples were assayed in a well-counter.

Data Analysis

General. Sinograms were corrected for attenuation using measured transmission data. Images were reconstructed using the software provided by the scanner manufacturer with 0.2 × 0.2 cm pixels using a Hann filter with cutoff 0.5 (0.148 mm^{-1}). Regions of interest (ROIs) were manually drawn on the [^{15}O]butanol and (S)- or (R)-[^{11}C]nicotine images by a physician experienced with PET images and knowledgeable in brain anatomy. ROIs and their abbreviated names are listed in Table 1. For the first nine regions listed in Table 1, regions were defined separately for the right and left hemispheres. Due to their small size relative to the image resolution and their proximity to midline, the thalami were difficult to separate visually, so one region was drawn encompassing both left and right thalami.

[^{15}O]Butanol. The uptake of [^{15}O]butanol was analyzed to determine cerebral perfusion (*17,18*). In this analysis, 40 sec of data were used beginning with the frame corresponding to the tissue takeoff time (*21*), which marks the arrival of the bolus in the brain. Tissue data were temporally aligned with the blood data according to the difference in tissue and blood takeoff times (*21*).

[^{11}C]Nicotine. Plasma radioactivity concentration was calculated from whole-blood radioactivity by using an assumed hematocrit of 0.4 and linear interpolation after low-pass filtering to reduce noise. Plasma radioactivity was then corrected for metabolites using the profile of Halldin et al. (*10*), which was linearly interpolated over the interval of 0–2 min and fit to a decaying exponential plus a constant for later times (0.237 + 0.728 $e^{-0.185(t-2)}$, t in min). The resultant curve was used as the model input function. Two models were considered in the data analysis: a three-compartment model and its simplification to a two-compartment model (Fig. 1). The compartment F of the three-compartment model corresponds to (S)- or (R)-[^{11}C]nicotine free in the tissue space as well as that which is nonspecifically associated with tissue components, whereas the compartment B represents nicotine specifically bound. The administered mass of (S)- or (R)-[^{11}C]nicotine was assumed to be sufficiently small so as to occupy a negligible fraction of the nicotinic binding sites. Also, radioactive metabolites were assumed not to enter the brain (*10*). Under these conditions, the time course of the molar concentration of (S)- or (R)-[^{11}C]nicotine in the compartments is described by

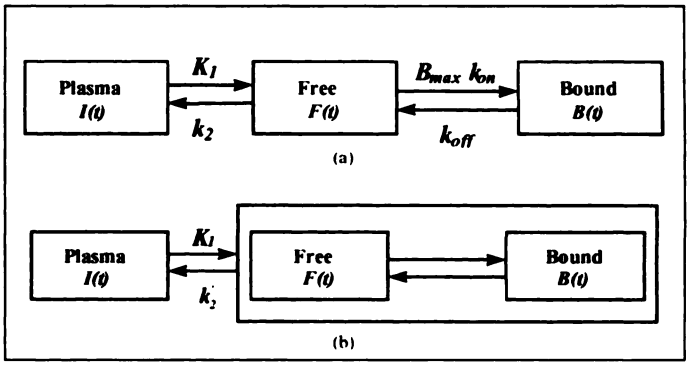

FIGURE 1. (A) Three-compartment model and (B) its two-compartment simplification.

$$\frac{dF}{dt} = K_1 I - k_2 F - k_{on} B_{max} F + k_{off} B$$

$$\frac{dB}{dt} = k_{on} B_{max} F - k_{off} B$$

where I(t) is the input function. The parameters K_1, k_2, k_{on}, k_{off} and B_{max} are the standard parameters used in PET receptor models, with B_{max} representing the concentration of unbound nicotinic binding sites at baseline. Because the administered mass of (S)- or (R)-[^{11}C]nicotine was small, the parameters k_{on} and B_{max} cannot be estimated separately; only their product may be estimated (*22*). Thus, the parameters $\theta = [K_1, k_2, k_{on}B_{max}, k_{off}]^T$ were estimated by using a Levenberg-Marquardt algorithm to minimize the weighted sum of squares difference between the measured tissue data for time frame i, PET(t_i), and the model predicted tissue radioactivity

$$\phi(\theta) = \sum_i w_i \left\{ PET(t_i) - S \int_{t_{i-1}}^{t_i} [(1 - F_v)(F + B) + F_v A]\, dt \right\}^2,$$

where S is the (time varying) specific activity; F_v is the assumed vascular fraction, 5%; and A is the whole-blood radioactivity concentration. F, B and I are measured in n*M* (equivalent to pmol/ml); PET and A are measured in MBq/ml. The weights, w_i, are defined as the reciprocal of the variance of the radioactivity estimate in the ROI (*23*). Estimates of the standard deviation of the parameter estimates were made as the square roots of the diagonal terms of the inverse of the Hessian matrix (*24*). Temporal alignment between the tissue and blood data was achieved by estimating a delay parameter for each region along with the other model parameters.

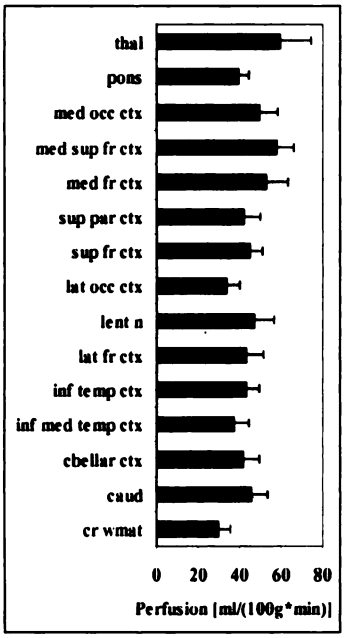

FIGURE 2. Baseline perfusion values measured with [^{15}O]butanol for five subjects. Error bars indicate 1 s.d.

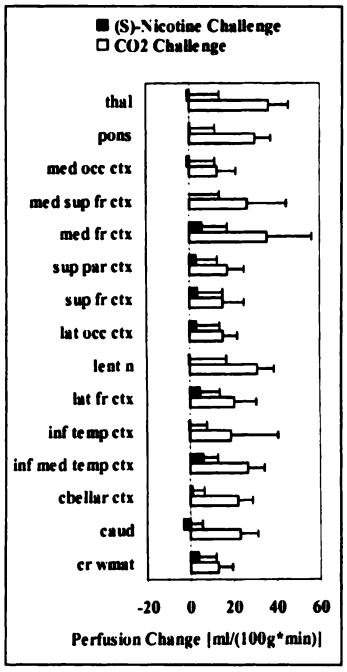

FIGURE 3. Perfusion changes from baseline due to CO_2 (two subjects) and (S)-nicotine challenge (five subjects). Error bars indicate 1 s.d.

For the two-compartment simplification of the three-compartment model, we assumed the association and dissociation of ligand to the binding sites occurred rapidly compared to the exchange across the blood–brain barrier. That is, the F and B compartments can be approximated as one well-mixed compartment (Fig. 1B). Mathematically, this implies that $B \approx F(k_{on}B_{max}/k_{off})$ (*25*) and that there are only two model parameters: K_1 and $k_2' = k_2/(1 + k_{on}B_{max}/k_{off})$. Also, k_2' may be expressed in terms of $k_D = k_{off}/k_{on}$: $k_2' = k_2/(1 + B_{max}/k_D)$. In the three-compartment model, the parameters related to nicotine binding, $k_{on}B_{max}$ and k_{off}, are independent of perfusion. In the two-compartment model, only the parameter k_2' is related to nicotine binding and this parameter is perfusion dependent because k_2 is perfusion dependent. [$K_1 = f(1 - e^{-PS/f})$ depends on blood flow f and the permeability surface product PS (*17*). Because K_1/k_2 equals the blood-to-brain partition coefficient that is independent of blood flow, k_2 is blood-flow dependent (*25*).] Therefore, we consider the composite parameter

$$DV = K_1/k_2' = \frac{K_1}{k_2}\left(1 + \frac{B_{max}}{k_D}\right)$$

that should be dependent on nicotine binding but that should be independent of perfusion because it equals the ratio of tissue-to-plasma concentration of tracer at steady state. It should be dependent on specific binding because the presence of other ligands will effectively reduce B_{max}, the concentration of binding sites available for binding to either (S)- or (R)-[^{11}C]nicotine.

Note that DV is equivalent to the parameter called DV″ by Koeppe et al. (*26*). Also, it is similar to the reciprocal of the parameter k_2^* of Nordberg et al. (*16*), except that the K_1 in the expression for k_2^* is that of butanol whereas the K_1 in the expression for DV is that of nicotine.

Some might argue that DV can be calculated simply as the ratio of tissue-to-blood concentrations at a late time point. However, such an estimate does not account for loss of tracer from the blood and therefore leads to biased estimates (*27,28*). An alternative would be a graphical method for DV determination. We chose to use a kinetic modeling approach because the data variance can be taken into account in the analysis. This is necessary to achieve optimal statistical properties of the parameter estimates.

RESULTS

Brain Perfusion

Regional perfusion values are displayed in Figure 2 for baseline conditions for the eight subjects. Averaged across all regions, perfusion measured with [^{15}O]butanol was 45.1 ± 8.2 ml/(100 g × min) (mean ± s.d.). Technical difficulties occurred in one of the CO_2 challenge brain perfusion studies. This dataset was therefore excluded from our analyses. Changes in regional perfusion values with CO_2 or (S)-nicotine challenge relative to baseline are presented in Figure 3. For all regions, perfusion increases from baseline were greater with CO_2 challenge than with (S)-nicotine challenge. Some regional perfusion decreases were observed but only with (S)-nicotine challenge. Analyzed as a set, the mean regional increase was 6.4 ± 3.1 ml/(100 g × min) with (S)-nicotine challenge compared to 36.5 ± 9.0 ml/(100 g × min) with CO_2 challenge. Analyzed individually using a one-tailed, paired t test, the regional perfusion increases with CO_2 challenge were significant ($p < 0.05$) in caudate, cerebellar cortex, inferior medial temporal cortex, lateral frontal cortex, lentiform nucleus and lateral occipital cortex. The increase was significant with (S)-nicotine challenge only in the inferior medial temporal cortex.

Carbon-11-Nicotine

A typical curve of whole-blood radioactivity after intravenous bolus of (S)-[^{11}C]nicotine is shown in Figure 4. Specific activity at injection time varied with the subject with a range of 12–58 GBq/μmol (320–1560 mCi/μmol). Images of brain (S)-[^{11}C]nicotine concentration averaged between 20 and 25 min are shown in Figure 5. With three-compartment analysis, parameter estimation often failed to converge. The value of k_{off} increased throughout the fitting until a numerical overflow

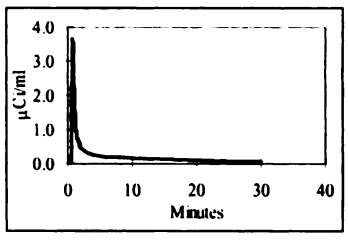

FIGURE 4. Arterial radioactivity concentration after intravenous bolus injection of 540 GBq (14.6 mCi) (S)-[^{11}C]nicotine into a 100-kg male subject.

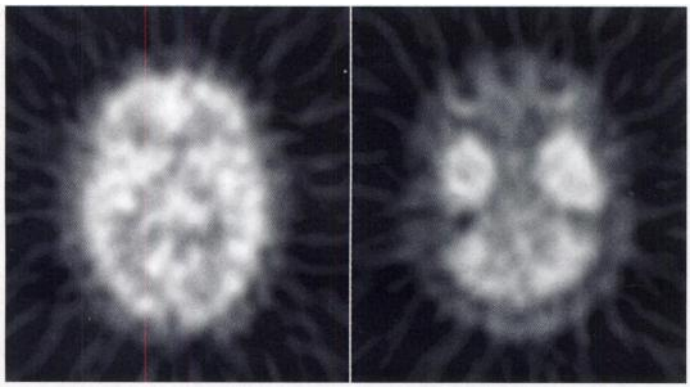

FIGURE 5. Images of (S)-[^{11}C]nicotine concentration averaged between 20 and 25 min after injection under baseline conditions.

occurred. In other cases, when convergence occurred, the estimate of k_{off} was typically greater than that of K_1 and k_2 and the model parameters were unidentifiable. That is, the effect of one parameter could not be distinguished experimentally from that of another. Moreover, the weighted sum of squared difference between the model and data was only marginally reduced using the more complex model (e.g., 30.6 versus 30.8 in Fig. 6A and 25.0 versus 25.0 in Fig. 6B). Consequently, comparisons of the two- and three-compartment models using the F test, the Akaike information criterion and the Schwarz criterion (*29*) all demonstrated that the more complex three-compartment model was not justified. This finding was consistent with our visual impression that the two-compartment model was adequate to fit the data (Fig. 6).

To assess whether metabolite correction is necessary, we also analyzed the tissue data without applying the metabolite correction to the input function. Without this correction, the rate constants of the model could not be adjusted so that the model-predicted radioactivity matched the rate of clearance of

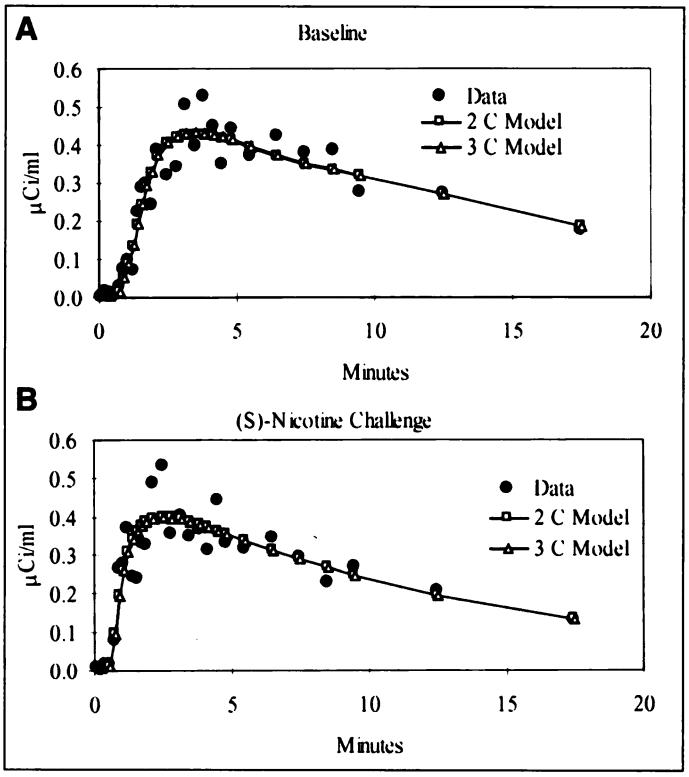

FIGURE 6. Comparison of model fits to (S)-[^{11}C]nicotine data using two- and three-compartment models for thalamus at (A) baseline and (B) after (S)-nicotine challenge.

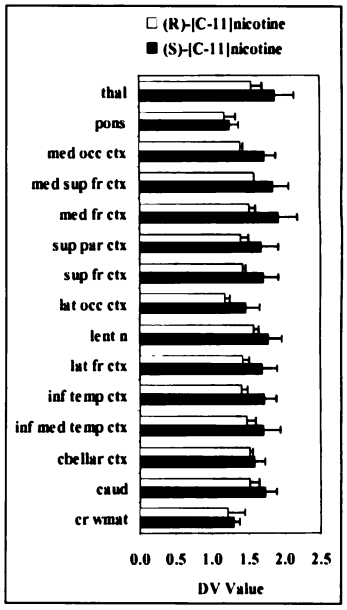

FIGURE 7. Baseline DV values for (S)-[^{11}C]nicotine (n = 6) and (R)-[^{11}C]nicotine (n = 2). Error bars indicate 1 s.d.

radioactivity from the tissue. Specifically, at late time points, the magnitude of the slope of the model-predicted radioactivity was less than that of the actual brain radioactivity. This lead to systematic differences between the model and data that were not present when the input function was corrected for metabolites as described previously.

Based on these findings, we concluded that the appropriate way to analyze the data was with a two-compartment model corrected for metabolites. With this approach, the parameter DV was expected to reflect specific binding. Accordingly, regional DV values are plotted in Figure 7. The mean regional (S)-[^{11}C]nicotine DV value of the six subjects was 1.67 ± 0.19 (unitless) at baseline. The mean regional (R)-[^{11}C]nicotine DV value of the two subjects was 1.42 ± 0.14 at baseline. In all regions, baseline DV values for (S)-[^{11}C]nicotine were greater than those for (R)-[^{11}C]nicotine and the difference was significant ($p < 0.05$, one-tailed, two-sample, unequal variance t test) in the inferior temporal cortex, lateral occipital cortex and superior frontal cortex. The difference was nearly significant ($p < 0.1$) in the caudate, medial occipital cortex, lateral frontal cortex and lentiform nucleus.

DV of both (R)- and (S)-[^{11}C]nicotine tended to decrease from baseline values with (S)-nicotine challenge (Fig. 8), whereas with CO_2 challenge, the effect on DV measured with (S)-[^{11}C]nicotine was more varied. The mean regional change from baseline in the (S)-[^{11}C]nicotine DV was −0.03 ± 0.04 with CO_2 challenge. The mean changes in DV with (S)-nicotine challenge were −0.15 ± 0.11 for (S)-[^{11}C]nicotine and −0.06 ± 0.06 for (R)-[^{11}C]nicotine. There was a significant regional variation in the changes that is reflected in these s.d. values. Analyzing these changes on a region-by-region basis, we found that (S)-nicotine challenge caused 14%, 15% and 23% reductions in DV of (S)-[^{11}C]nicotine from baseline in the caudate, lentiform nucleus and thalamus, respectively, which were highly significant ($p < 0.01$, one-tailed, paired t test) (Table 2). Reductions of 10%, 8%, 8%, 9% and 8% in the cerebellar cortex, inferior temporal cortex, lateral frontal cortex, superior frontal cortex and medial superior frontal cortex also achieved statistical significance ($p < 0.05$). The 14% reduction in the pons was nearly significant ($p = 0.053$). (S)-nicotine challenge caused significant ($p < 0.05$) decreases in (R)-[^{11}C]nicotine DV in the inferior temporal cortex and thalamus, 2% and 9%, respectively, and nearly significant decreases in the

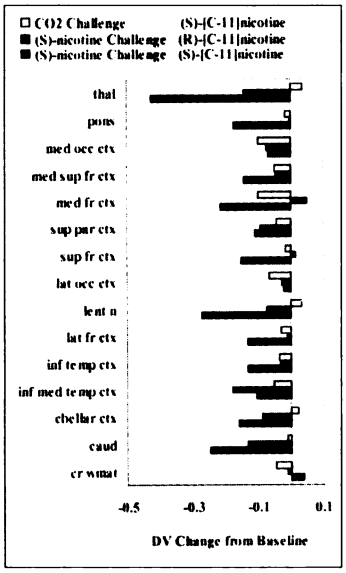

FIGURE 8. DV changes from baseline due to CO_2 (n = 2) and (S)-nicotine challenge (n = 2 for (R)-[^{11}C]nicotine, n = 3 for (S)-[^{11}C]nicotine). For visual clarity, the error bars are not shown.

medial superior frontal cortex (p = 0.064) and the medial occipital cortex (p = 0.073), 3% and 5%, respectively. There were no regions with statistically significant DV changes with CO_2 challenge; all p values were greater than 0.10 (Table 2).

To estimate the fraction of binding sites occupied by (S)-nicotine challenge, we analyzed the data from one subject as follows. The thalamus concentration of (S)-[^{11}C]-nicotine was 0.4 n*M* in the scan collected between 20 and 25 min postinjection. Assuming that the 1000-fold greater mass of the (S)-nicotine in the challenge distributed similarly to its labeled counterpart that was injected separately, the tissue concentration (S)-nicotine was estimated as 400 n*M*. We set F + B to this value and used the equilibrium relation $B/B_{max} = F/(k_D + F)$ to estimate (S)-nicotine binding. Considering the high-affinity nicotinic binding sites with k_D = 8.1 n*M* (*30*), B_{max} = 36 fmol/mg protein (*30*), and assuming the brain is 10% protein (*31*), we estimated that 98% of the binding sites available to (S)-nicotine were occupied by it. Moreover, even if only one fourth of the (S)-nicotine in the tissue had access to the binding sites, the occupancy would be 90%. Thus, we believe the (S)-nicotine challenge led to a significant occupancy of binding sites by (S)-nicotine.

Our intent was to use high specific activity (S)- or (R)-[^{11}C]nicotine to minimize the fraction of available binding sites occupied by the radioligand. In these experiments, the lowest specific activity was 12 GBq/μmol (320 mCi/μmol). For this specific activity, we estimated an upper limit on the fraction of binding sites occupied by the radioligand as follows. Using data from paired baseline and (S)-nicotine challenge studies and assuming that essentially all binding sites were occupied by (S)-nicotine in the challenge study, we estimated B_{max}/k_D as $(DV_{baseline} - DV_{challenge})/DV_{challenge}$. The maximum observed value for B_{max}/k_D occurred in the thalamus and was 0.49 (mean = 0.097, s.d. = 0.12). This value was used to estimate $B/F \approx B_{max}/k_D$ (see Data Analysis section), which we then used to estimate the fraction of tissue radioactivity attributable to specifically bound radioligand, $B/(F + B) \approx B_{max}/k_D/(1 + B_{max}/k_D)$, wherein vascular radioactivity was neglected. Substituting the value $B_{max}/k_D = 0.49$ into this expression reveals that the maximum specific uptake fraction was approximately one third. For this study, thalamic uptake of radioligand between 20 and 25 min postinjection in the baseline scan was 0.73 n*M*, of which one third, 0.24 n*M*, was attributed to specific binding. This represented only about 1% of the 23.1 n*M* of thalamic binding sites measured in vitro (*31,32*). From these considerations, we conclude that neglecting the occupancy of binding sites by the radioligand in the kinetic analysis is appropriate.

DISCUSSION

Brain Perfusion

It is interesting to note that there was an increase in perfusion with (S)-nicotine challenge (Fig. 3). Perhaps this effect explains the perfusion changes (*33*) and is a reflection of the improvement in cognitive and psychomotor function (*34–36*) reported with cigarette smoking.

Carbon-11-Nicotine

Model Configuration. In Figure 6, we display the data and model tissue radioactivity curves for the thalamus. This is the

TABLE 2
Summary Statistics

Name	Abbreviation	Significance of distribution volume change from baseline (p value)		
		(S)-[^{11}C]Nicotine		(R)-[^{11}C]Nicotine
		CO_2 challenge	(S)-Nicotine challenge	(S)-Nicotine challenge
Caudate	caud	0.463	0.006**	0.331
Cerebellar cortex	cbellar ctx	0.184	0.011*	0.187
Inferior medial temporal cortex	inf med temp ctx	0.309	0.209	0.013*
Inferior temporal cortex	inf temp ctx	0.242	0.024*	0.160
Lateral frontal cortex	lat fr ctx	0.289	0.016*	0.393
Lentiform nucleus	lent n	0.191	0.007**	0.441
Lateral occipital cortex	lat occ ctx	0.125	0.300	0.150
Superior frontal cortex	sup fr ctx	0.358	0.038*	0.340
Superior parietal cortex	sup par ctx	0.275	0.093	0.378
Medial frontal cortex	med fr ctx	0.174	0.123	0.173
Medial superior frontal cortex	med sup fr ctx	0.362	0.015*	0.064
Medial occipital cortex	med occ ctx	0.289	0.217	0.073
Corona radiata (white matter)	cr wmat	0.340	0.282	0.328
Pons	pons	0.359	0.053	0.491
Thalamus	thal	0.351	0.007**	0.039*

*significant, $p < 0.05$; **highly significant, $p < 0.01$.

region with the greatest DV decrease from baseline with (S)-nicotine challenge and therefore would be the region most likely to demonstrate inadequacies of the two-compartment model if any exist. For the baseline and (S)-nicotine challenge data, the fits obtained using the three-compartment model were not significantly better than those obtained using the two-compartment model.

In their three-compartment analysis, Nybäck et al. (*15*) found no indication of specific binding. This is consistent with our results with three-compartment analysis. We found that use of the more complex model was not justified by the data. However, we believe this is due to the rapid association and dissociation of (S)-nicotine, which made the specific binding kinetically indistinguishable from nonspecific uptake.

DV as an index of specific binding. DV is an appropriate parameter for assessing changes in specific binding. DV was affected by (S)-nicotine challenge. These changes could not be attributed to changes in perfusion because perfusion changes associated with CO_2 challenge, which were greater than those observed with (S)-nicotine challenge, failed to cause significant changes in DV.

We prefer to quantify specific nicotine binding using DV instead of k_2^* (*16*) for the following reasons. Although k_2^* is similar in nature to the reciprocal of DV, there is an important distinction: k_2^* is equal to DV times the ratio of the single-pass extraction fraction of butanol to that of nicotine. It is only when the extraction fractions are equal that the measures are equivalent. In comparison, by using DV, we avoid this potential pitfall. Moreover, whereas DV can be determined from a single PET study, k_2^* unnecessarily complicates the data acquisition by additionally requiring a butanol scan. In addition, K_1 and k_2 parameter estimates are inherently correlated such that their ratio can be more precisely determined than the individual terms. Thus, the precision of k_2^* that is calculated as the ratio of k_2 from one scan to that of K_1 from another scan will be poorer than the precision of DV. Therefore, estimates of DV should be more precise than k_2^* estimates.

As further support for the use of DV to quantify specific nicotine binding, we note that not only is the direction of the observed changes in DV consistent with specific binding, but the magnitudes of the changes are consistent with the regional concentrations of binding sites. In particular, we observed a factor of two difference between the reduction in DV of (S)-[^{11}C]nicotine induced by (S)-nicotine in the temporal cortex from that in the thalamus. This is consistent with the twofold difference in nicotinic binding sites in these areas (*36*).

Apparent Contradiction in the Literature. Our finding that there is PET-observable specific binding of (S)-[^{11}C]nicotine is consistent with a report by Nordberg et al. (*16*), who have also quantified (S)-[^{11}C]nicotine binding in the brain and found it to be negatively correlated with cognitive function and presumably the severity of Alzheimer's disease.

Our work adds valuable insight into how such studies should be designed in the future. First, we established that there is a problem of a high level of free and/or nonspecifically bound [^{11}C]nicotine. This unfortunately means that [^{11}C]nicotine is a relatively poor tracer for assessing specific nicotinic binding with PET. Second, we introduced the use of DV to quantify specific nicotine binding and demonstrated that DV is not affected by changes in perfusion. Third, we demonstrated that 20-min data segments can be reliably analyzed using the two-compartment model. In comparison, Nordberg et al. (*16*) used only 4–5 min of data. Because the effects of perfusion are more pronounced early in the study, the use of the longer interval may increase the relative sensitivity to changes in the status of nicotinic binding sites.

On the surface, our findings appear to be discordant with those of Nybäck et al. (*14*), who found that the tissue uptake curves of (S)-[^{11}C]nicotine were not altered by excess (S)-nicotine given concomitantly with the tracer or given 7 min after the tracer. Indeed, because the specific binding of (S)-[^{11}C]nicotine is a small component of its brain uptake, specific uptake is easily overlooked. Nevertheless, our data indicate that specific binding, although subtle, is detectable with PET.

Nybäck et al. (*14*) concluded that the early brain uptake of (S)-[^{11}C]nicotine was "mainly determined by the cerebral blood flow, extraction of the tracer over the blood-brain barrier and unspecific binding." This conclusion is not inconsistent with our data in which values of K_1 for (S)-nicotine were similar in magnitude to those of a highly extracted, freely diffusible tracer. However, in itself, this is not sufficient to rule out the possibility that (S)-[^{11}C]nicotine might be useful for assessing specific binding. In particular, it is possible that a tracer could provide good estimates of the perfusion-extraction product (K_1) as well as specific binding (DV). For DV to be sensitive to specific binding, specific uptake needs to be a significant fraction of brain uptake. Our data show that a (S)-nicotine challenge that probably blocked nearly all available binding sites induced only an 8%–23% reduction in DV. Thus, we establish that specific binding comprises a small fraction of tissue uptake and conclude that (S)-[^{11}C]nicotine is a relatively poor tracer for assessing specific nicotinic binding with PET.

Our results differed from those of Nybäck et al. (*14*) in that Nybäck et al. observed K_1 and k_2' values that were higher at high specific activity than at low specific activity. For comparison with the present work, we calculated DV values from these published K_1 and k_2' values for (S)-[^{11}C]nicotine (Table 2) (*15*). If specific binding did not occur, DV would be the same for both high- and low-specific-activity studies. If specific binding did occur, one would expect the DV values measured in the low-specific-activity experiment to be lower than those measured in the high-specific-activity experiment. Consistent with specific binding, thalamus DV values obtained from low-specific-activity experiments were lower than those from high-specific-activity experiments. However, the published data for the other regions were inconsistent with our observations and showed an unexpected pattern: The DV values in the low-specific-activity study were higher than in the high-specific-activity study. We can think of no explanation for this behavior. Nybäck et al. (*14*) postulated competition (i.e., active or facilitated transport) between labeled and unlabeled nicotine at the blood–brain barrier. We are not aware of any mechanism for active or facilitated transport of nicotine across the blood–brain barrier.

In summary, the apparent contradiction in the conclusions of Nordberg et al. (*16*) and Nybäck et al. (*14*) can be explained in light of our data as follows. Only a small component of (S)-nicotine uptake represents specific binding. Whether it can be detected is probably dependent on the details of the data acquisition and analysis. For these reasons, (S)-[^{11}C]nicotine does not have ideal properties for assessing the status of nicotinic binding sites with PET.

Enantiomeric Specificity

The baseline DV values for (S)-[^{11}C]nicotine were greater than those for (R)-[^{11}C]nicotine (Fig. 7). In addition, the regions in which and the degree to which the DV of (R)-[^{11}C]nicotine and (S)-[^{11}C]nicotine were reduced by (S)-nicotine challenge were different (Table 2). Taken together, these results are

consistent with other reports (*10,11,14*) that indicate that the affinity and/or concentration of binding sites is different for (R)-[^{11}C]nicotine and (S)-[^{11}C]nicotine. However, it is important to note that we found evidence of specific binding of both (R)-[^{11}C]nicotine and (S)-[^{11}C]nicotine (Table 2) because (S)-nicotine challenge caused statistically significant regional decreases in DV for each enantiomer.

CONCLUSION

Specific binding of (R)- and (S)-[^{11}C]nicotine were detected using the perfusion-independent parameter DV. However, because large changes in specific binding were reflected by small changes in DV, we conclude that (R)- and (S)-[^{11}C]nicotine are rather poor tracers for assessing the status of nicotinic binding sites.

ACKNOWLEDGMENTS

A subset of this work was presented verbally at the Society of Nuclear Medicine Annual Meeting, June 1996, Denver, Colorado. We sincerely appreciate the insightful comments of anonymous reviewers that have lead to improvements in the article. We thank B. Bennington and E. Wilson for radioligand preparation and G.P. Leisure for PET scanning. We are grateful to E. Morris for proofreading an early version of the article. This work was supported, in part, by Philip Morris USA. The Whitaker Foundation supported PET modeling efforts of Raymond F. Muzic, Jr. and Ning Zhu.

REFERENCES

1. Aubert I, Araujo DM, Cecyre D, Robitaille Y, Gauthier S, Quirion R. Comparative alterations of nicotinic and muscarinic binding sites in Alzheimer's and Parkinson's diseases. *J Neurochem* 1992;58:529–541.
2. Benwell ME, Balfour DJ, Anderson JM. Evidence that tobacco smoking increases the density of (−)-[^{3}H]nicotine binding sites in human brain. *J Neurochem* 1988;50:1243–1247.
3. Nordberg A, Winblad B. Reduced number of [^{3}H]nicotine and [^{3}H]acetylcholine binding sites in the frontal cortex of Alzheimer brains. *Neurosci Lett* 1986;72:115–119.
4. Kellar KJ, Whitehouse PJ, Martino-Barrows AM, Marcus K, Price DL. Muscarinic and nicotinic cholinergic binding sites in Alzheimer's disease cerebral cortex. *Brain Res* 1987;436:62–68.
5. Whitehouse PJ, Martino AM, Wagster MV, et al. Reductions in [^{3}H]nicotinic acetylcholine binding in Alzheimer's disease and Parkinson's disease: an autoradiographic study. *Neurology* 1988;38:720–723.
6. Nordberg A, Adem A, Hardy J, Winblad B. Change in nicotinic receptor subtypes in temporal cortex of Alzheimer brains. *Neurosci Lett* 1988;86:317–321.
7. Adem A, Jossan SS, d'Argy R, Brandt I, Winblad B, Nordberg A. Distribution of nicotinic receptors in human thalamus as visualized by ^{3}H-nicotine and ^{3}H-acetylcholine receptor autoradiography. *J Neural Transm* 1988;73:77–83.
8. Whitehouse PJ, Kalaria RN. Nicotinic receptors and neurodegenerative dementing diseases: basic research and clinical implications. *Alzheimer Dis Assoc Disord* 1995;9(suppl 2):3–5.
9. Långström B, Antoni G, Gullberg P, et al. Synthesis of L- and D-[methyl-^{11}C]methionine. *J Nucl Med* 1987;28:1037–1040.
10. Halldin C, Nagren K, Swahn CG, Långström B, Nybäck H. (S)- and (R)-[^{11}C]nicotine and the metabolite (R/S)-[^{11}C]cotinine. Preparation, metabolite studies and in vivo distribution in the human brain using PET. *Int J Rad Appl Instrum [B]* 1992;19:871–880.
11. Nordberg A, Hartvig P, Lilja A, et al. Decreased uptake and binding of ^{11}C-nicotine in brain of Alzheimer patients as visualized by positron emission tomography. *J Neural Transm Park Dis Dement Sect* 1990;2:215–224.
12. Nordberg A, Lilja A, Lundqvist H, et al. Tacrine restores cholinergic nicotinic receptors and glucose metabolism in Alzheimer patients as visualized by positron emission tomography. *Neurobiol Aging* 1992;13:747–758.
13. Nordberg A, Hartvig P, Lilja A, et al. Nicotine receptors in the brain of patients with Alzheimer's disease. Studies with ^{11}C-nicotine and positron emission tomography. *Acta Radiol* 1991;376(suppl)165–166.
14. Nybäck H, Nordberg A, Långström B, et al. Attempts to visualize nicotinic receptors in the brain of monkey and man by positron emission tomography. *Prog Brain Res* 1989;79:313–319.
15. Nybäck H, Halldin C, Ahlin A, Curvall M, Eriksson L. PET studies of the uptake of (S)- and (R)-[^{11}C]nicotine in the human brain: difficulties in visualizing specific receptor binding in vivo. *Psychopharmacology (Berl)* 1994;115:31–36.
16. Nordberg A, Lundqvist H, Hartvig P, Lilja A, Långström B. Kinetic analysis of regional (S)(−)^{11}C-nicotine binding in normal and Alzheimer brains—in vivo assessment using positron emission tomography. *Alzheimer Dis Assoc Disord* 1995;9:21–27.
17. Herscovitch P, Raichle ME, Kilbourn MR, Welch MJ. Positron emission tomographic measurement of cerebral blood flow and permeability-surface area product of water using [^{15}O]water and [^{11}C]butanol. *J Cereb Blood Flow Metab* 1987;7:527–542.
18. Berridge MS, Adler LP, Nelson AD, et al. Measurement of human cerebral blood flow with [^{15}O]butanol and positron emission tomography. *J Cereb Blood Flow Metab* 1991;11:707–715.
19. Wienhard K, Eriksson L, Grootoonk S, Casey M, Pietrzyk U, Heiss WD. Performance evaluation of the positron scanner ECAT EXACT. *J Comput Assist Tomogr* 1992;16:804–813.
20. Nelson AD, Muzic RF Jr, Miraldi F, Muswick GJ, Leisure GP, Voelker W. Continuous arterial positron monitor for quantitation in PET imaging. *Am J Physiol Imaging* 1990;5:84–88.
21. Muzic RF Jr, Nelson AD, Miraldi F. Temporal alignment of tissue and arterial data and selection of integration start times for the $H_2{}^{15}O$ autoradiographic CBF model in PET. *IEEE Trans Med Imag* 1993;12:393–398.
22. Mintun MA, Raichle ME, Kilbourn MR, Wooten GF, Welch MJ. A quantitative model for the in vivo assessment of drug binding sites with positron emission tomography. *Ann Neurol* 1984;15:217–227.
23. Huesman RH. A new fast algorithm for the evaluation of regions of interest and statistical uncertainty in computed tomography. *Phys Med Biol* 1984;29:543–552.
24. Muzic RF Jr, Nelson AD, Saidel GM, Miraldi F. Optimal experiment design for PET quantification of receptor concentration. *IEEE Trans Med Imaging* 1996;15:2–12.
25. Logan J, Volkow ND, Fowler JS, et al. Effects of blood flow on [^{11}C]rac pride binding in the brain: model simulations and kinetic analysis of PET data. *J Cereb Blood Flow Metab* 1994;14:995–1010.
26. Koeppe RA, Holthoff VA, Frey KA, Kilbourn MR, Kuhl DE. Compartmental analysis of [^{11}C]flumazenil kinetics for the estimation of ligand transport rate and receptor distribution using positron emission tomography. *J Cereb Blood Flow Metab* 1991;11:735–744.
27. Logan J, Fowler JS, Volkow ND, et al. Graphical analysis of reversible radioligand binding from time-activity measurements applied to [N-^{11}C-methyl]-(−)-cocaine PET studies in human subjects. *J Cereb Blood Flow Metab* 1990;10:740–747.
28. Carson RE, Channing MA, Blasberg RG, et al. Comparison of bolus and infusion methods for receptor quantitation: application to [^{18}F]cyclofoxy and positron emission tomography. *J Cereb Blood Flow Metab* 1993;13:24–42.
29. Landaw EM, DiStefano JJ. Multiexponential, multicompartmental, and noncompartmental modeling. II. Data analysis and statistical considerations. *Am J Physiol* 1984;246:R665–R677.
30. Shimohama S, Taniguchi T, Fujiwara M, Kameyama M. Biochemical characterization of the nicotinic cholinergic receptors in human brain: binding of (−)-[3H]nicotine. *J Neurochem* 1985;45:604–610.
31. Soderberg M, Edlund C, Alafuzoff I, Kristensson K, Dallner G. Lipid composition in different regions of the brain in Alzheimer's disease/senile dementia of Alzheimer's type. *J Neurochem* 1992;59:1646–1653.
32. Nordberg A, Alafuzoff I, Winblad B. Nicotinic and muscarinic subtypes in the human brain: changes with aging and dementia. *J Neurosci Res* 1992;31:103–111.
33. Silvestrini M, Troisi E, Matteis M, Cupini LM, Bernardi G. Effect of smoking on cerebrovascular reactivity. *J Cereb Blood Flow Metab* 1996;16:746–749.
34. Pritchard WS, Robinson JH, deBethizy JD, Davis RA, Stiles MF. Caffeine and smoking: subjective, performance, and psychophysiological effects. *Psychophysiology* 1995;32:19–27.
35. Sherwood N. Effects of cigarette smoking on performance in a simulated driving task. *Neuropsychobiology* 1995;32:161–165.
36. Levin ED, Rose JE. Nicotinic and muscarinic interactions and choice accuracy in the radial-arm maze. *Brain Res Bull* 1991;27:125–128.